

1 **Title**

2 Can sonic tomography predict loss in load-bearing capacity for trees with internal defects? A  
3 comparison of sonic tomograms with destructive measurements

4  
5 **Authors**

6 Daniel C. Burcham<sup>1\*</sup>, Nicholas J. Braze<sup>2</sup>, Robert E. Marra<sup>3</sup>, and Brian Kane<sup>4</sup>

7  
8 <sup>1</sup>Centre for Urban Greenery and Ecology

9 National Parks Board

10 Singapore 259569

11

12 <sup>2</sup>Center for Agriculture, Food, and the Environment

13 University of Massachusetts Amherst

14 Amherst, MA 01003

15

16 <sup>3</sup>Department of Plant Pathology and Ecology

17 Connecticut Agricultural Experiment Station

18 New Haven, CT 06504

19

20 <sup>4</sup>Department of Environmental Conservation

21 University of Massachusetts Amherst

22 Amherst, MA 01003

23

24 \*Corresponding author: [daniel\\_christopher\\_burcham@nparks.gov.sg](mailto:daniel_christopher_burcham@nparks.gov.sg); +65 6465 6950

25

26 **Acknowledgments**

27 Funding for tomography and destructive measurements was provided by the National Science

28 Foundation EARly-Concept Grants for Exploratory Research (EAGER) Program (Grant #DEB-

1 1346258. Additional funding for numerical analysis was provided by the National Parks Board,  
2 Singapore.

3

#### 4 **Key message**

5 Sonic tomography can be used to examine reductions in the load-bearing capacity of tree parts with  
6 internal defects, but the limitations of sonic tomography and mathematical methods must be  
7 considered.

8

#### 9 **Abstract**

10 The measurement and assessment of internal defects is an important aspect of tree risk assessment.  
11 Although there are several methods for estimating the reduced load-bearing capacity of trees with  
12 internal defects, the advancement of these methods has not kept pace with improvements to methods  
13 used to measure the internal condition of trees, such as sonic tomography. In this study, the percent  
14 reduction to the section modulus,  $Z_{LOSS}$  (%), caused by internal defects was estimated using 51 sonic  
15 tomograms collected from three tree species, and the accuracy of measurements was assessed using  
16 the destructively measured internal condition of the corresponding cross sections. In tomograms, there  
17 was a repeated underestimation of the percent total damaged area,  $A_D$  (%), and a repeated  
18 overestimation of the offset distance between the centroid of the trunk and the centroid of the largest  
19 damaged part,  $L_O$  (m). As a result,  $Z_{LOSS}$  determined using tomograms was mostly less, in absolute  
20 terms, than determined from destructive measurements. However, the accuracy of these estimates  
21 improved when using colors associated with intermediate sonic velocities to select damaged parts in  
22 tomograms, in addition to the colors explicitly associated with the slowest sonic velocities. Among  
23 seven mathematical methods used to estimate  $Z_{LOSS}$ , those accounting for  $L_O$  were more accurate than  
24 others neglecting it. In particular, a numerical method incorporating greater geometric detail, called  
25 *zloss*, gave estimates that were consistently better than six other analytical methods.

26

#### 27 **Author Contribution Statement**

1 DB and BK conceived and designed the study, NB and RM collected the data, DB analyzed data and  
2 wrote the manuscript, and all authors edited the manuscript.

3

#### 4 **Conflict of Interest**

5 The authors declare that they have no conflict of interest.

6

#### 7 **Introduction**

8 Several formulas have been used to estimate the strength loss (i.e., loss in load-bearing capacity)  
9 caused by internal defects in living trees, and most are based on the difference in the second moment  
10 of area,  $I$  ( $m^4$ ), between a hollow and solid trunk section (Kane et al. 2001).  $I$  represents the load-  
11 bearing capacity of a shape where the contribution of a material element to a total bending moment is  
12 proportional to the square of its distance ( $y$ ) from the neutral axis (Ennos 2012); it can be determined  
13 by summing the many, infinitesimally small moments distributed over a cross section of area ( $A$ ):

$$14 \quad I = \int y^2 dA. \quad \text{Eq. 1}$$

15 Practically, this means that wood situated near the trunk periphery contributes greater to overall  
16 rigidity. Coder (1989) used the formula to estimate the percent loss in  $I$ ,  $I_{LOSS}$  (%), of a hollow pipe  
17 relative to a solid rod:

$$18 \quad I_{LOSS} = d^4 / D^4, \quad \text{Eq. 2}$$

19 where  $d$  and  $D$  are the diameters of hollow and solid circles, respectively. Wagener (1963) modified  
20 this formula as the cube of the same ratio:

$$21 \quad I_{LOSS} = d^3 / D^3. \quad \text{Eq. 3}$$

22 It is unclear why Wagener (1963) chose this specific exponent. Most observe that it produces a larger  
23 and more conservative estimate over the range of possible  $d/D$  (Ciftci et al. 2014, Kane et al. 2001),  
24 but he implied that it offered a coarse approximation of strength loss, presumably as a compromise  
25 between the geometric properties governing bending stress ( $I \propto D^4$ ) and compression stress ( $A \propto D^2$ )  
26 (Wagener 1963). Later, Smiley and Fraedrich (1992) modified this formula to approximate trees with  
27 open cavities as a sector of a circular annulus:

1 
$$I_{LOSS} = d^3/D^3 + R(D^3 - d^3)/D^3, \quad \text{Eq. 4}$$

2 where  $R$  is the ratio of cavity opening to stem circumference. For trees without a cavity opening,  
3 estimates given by Eq. 4 are identical to Eq. 3. Among the three formulas, only the latter was  
4 validated with empirical data (Smiley and Fraedrich 1992).

5

6 However, several limitations of these formulas diminish their applicability to many common  
7 situations. The formulas are appropriate for circular cylinders composed of isotropic, homogeneous  
8 material, and Wagener's (1963) and Coder's (1989) implicitly assume concentric areas of decay in  
9 which the decayed and solid areas share the same centroid. A circle is often an inexact approximation  
10 of the shape of a tree, especially near the base of those with pronounced buttress roots, and circles  
11 frequently do not accurately describe the shape of decayed areas. In addition, decay is often formed  
12 asymmetrically so that its centroid is offset from that of the trunk, and these formulas ignore the  
13 potentially significant contributions of offset decayed areas (Kane and Ryan 2004).

14

15 To address these limitations, Ciftci et al. (2014) used the section modulus,  $Z$  ( $\text{m}^3$ ), to evaluate the loss  
16 in load-bearing capacity, taken as moment capacity, due to decay:

17 
$$Z = I/y, \quad \text{Eq. 5}$$

18 where  $y$  is the maximum perpendicular distance (m) between the neutral axis and outermost trunk  
19 fibers. The ratio is needed to calculate bending stress,  $\sigma$  ( $\text{N}\cdot\text{m}^{-2}$ ), for beams, or beam-like plant organs  
20 (Niklas 1992):

21 
$$\sigma = My/I, \quad \text{Eq. 6}$$

22 where  $M$  ( $\text{N}\cdot\text{m}$ ) is a bending moment causing rotation about the neutral axis. Eq. 6 shows that, for any  
23 loading situation, the maximum stress experienced by a cross section of any shape can be minimized  
24 by maximizing  $Z$  (Niklas 1992). Ciftci et al. (2014) estimated the percent loss in  $Z$ ,  $Z_{LOSS}$  (%), between  
25 a solid and hollow trunk section, and considered cases with both concentric and non-concentric  
26 decayed areas. The authors also considered the effects of material anisotropy on  $Z_{LOSS}$ , which was  
27 negligible (Ciftci et al. 2014).

1

2 Many of the limitations associated with existing strength-loss formulas arise from the unavailability of  
3 analytical solutions to the moments of irregular shapes (Ciftei et al. 2014, Kane et al. 2001), but  
4 numerical approaches can be used to compute these values for any shape (Koizumi and Hirai 2006).

5 Numerical analysis could address many of the limitations associated with existing approaches to  
6 estimating strength loss, including irregular geometry and non-concentric decayed areas, but this  
7 would require an accurate description of the size, position, and shape of decay in a trunk cross section.

8

9 Among consulting arborists, sonic tomography (SoT) is increasingly recognized as a useful way to  
10 evaluate the internal condition of trees (Smiley et al. 2011), offering reasonably accurate, non-  
11 invasive, and convenient assessments of the internal condition of the tree (Johnstone et al. 2010).

12 Sonic tomography measures variation in acoustic transmission speeds, which is proportional to the  
13 ratio of wood stiffness to density (Arciniegas et al. 2014). The advantages and limitations of SoT have  
14 been documented by several studies (Brazee et al. 2011, Li et al. 2012, Ostrovsky et al. 2017, Wang et  
15 al. 2009). Although SoT generally depicts the internal condition of trees accurately, some authors  
16 reported that measurements often underestimate the size of decayed areas (Liang et al. 2007, Wang et  
17 al. 2009), overestimate the size of cracks (Wang et al. 2007), and suffer inaccuracies on irregularly  
18 shaped trunks (Gilbert et al. 2016). Notwithstanding these minor shortcomings, sonic tomography is a  
19 natural choice to provide the raw data necessary for a numerical approach to estimating the loss in  
20 load-bearing capacity of trees with internal defects. In this study, existing analytical methods for  
21 estimating  $Z_{LOSS}$  were compared to a numerical estimate derived from sonic tomograms. The method  
22 was validated by applying it to sonic tomograms and the corresponding cross-sectional photographs  
23 from a previous study (Marra et al. 2018), in which trees were destructively harvested to assess the  
24 accuracy of interpretations derived from sonic tomograms.

25

26 The specific objectives of this study were to: (i) compare estimates of internal damage in three  
27 hardwood species provided by SoT with internal damage measured on destructively sampled trees; (ii)  
28 compare analytical and numerical estimates of strength loss derived from SoT and destructively

1 sampled trees; and (iii) test whether geometric features of damaged parts (i.e., size, position, shape)  
2 affect the accuracy of different approaches to estimating strength loss.

#### 4 **Materials and methods**

##### 5 *Site and tree material*

6 All tomograms and corresponding cross-sectional photographs used for this study were obtained from  
7 a previous study in which the accuracy of tomographic predictions was assessed by destructive  
8 sampling (Marra et al. 2018). In 2014, individuals of three species [American beech (AB, *Fagus*  
9 *grandifolia*); sugar maple (SM, *Acer saccharum*); and yellow birch (YB, *Betula alleghaniensis*)] were  
10 chosen based on the appearance of internal decay. Trees were assessed using the PiCUS® Sonic  
11 Tomograph 3 (Argus Electronic GmbH, Rostock, Germany) at one to four levels on the lower trunk,  
12 with the lowest cross section typically positioned 50 cm above the soil line. Tomograms display the  
13 relative sound transmission speeds on a colorimetric scale: the greatest sonic transmission speeds,  
14 associated with non-decayed wood, are depicted using varying shades of brown; decreasing speeds  
15 associated with lower density-specific stiffness, and more advanced stages of decay, are depicted, in  
16 order, as green, violet, and blue (Figure 1B). After felling trees, cross sections corresponding with  
17 each tomogram were excised from the trunk and photographed (Figure 1C). For this study, only cross  
18 sections with internal defects detected by SoT were used for analysis. See Marra et al. (2018) for more  
19 details.

##### 21 *Image analysis*

22 Three separate image files were used for analysis: a geometry image showing only the blue trunk  
23 boundary line (Figure 1A), a sonic tomogram showing the visualized decay pattern (Figure 1B), and a  
24 reference photograph of the tree's destructively measured internal condition (Figure 1C). The  
25 geometry and tomogram images were oriented identically without annotation and exported as JPEG  
26 files from the PiCUS® software. The size of the exported images was  $770 \times 770$  pixels.

1 A tomogram is displayed by the PiCUS® software in a Cartesian coordinate plane. To extract  
2 boundary coordinates for the solid and damaged parts, an object was created to relate the intrinsic  
3 coordinates of the tomogram images to the spatial coordinates of a Cartesian coordinate system.  
4 Similarly, the recorded distances between measurement points on each trunk were used to relate the  
5 intrinsic coordinates of the reference photographs to a Cartesian coordinate system. These objects  
6 used the calculated physical extent of each pixel to convert a pixel index (row, column) to a  
7 coordinate pair (x, y).

8  
9 The geometry and tomogram images were segmented using specific ranges in the hue, saturation,  
10 brightness (HSV) and LAB color space, respectively (Table 1). Each sonic tomogram was segmented  
11 to select either violet and blue (VB) or green, violet, and blue (GVB). This distinction between color  
12 combinations was made because the PiCUS® software excludes green areas when calculating the  
13 percent solid and damaged area in tomograms, but all parts of the cross section need to be classified as  
14 either solid or damaged for  $Z_{LOSS}$  calculations.

15  
16 Reference images of each tree's destructively measured internal condition were manually binarized  
17 into black (0) and white (1) images using Adobe Photoshop CS6 Extended (Adobe Systems, Inc., San  
18 Jose, California, United States) in which black and white, respectively, represented damaged and solid  
19 parts (Figure 1D). The trunk boundary, excluding bark, was used to define an enclosed region of  
20 interest, and the extent of damaged parts was determined visually by the presence of discoloration,  
21 cavities, cracks, and decayed wood. Wood discolored by the host defensive response and heartwood  
22 formation were classified as solid parts. Visual identification of damaged parts in cross sections is  
23 consistent with most existing studies (Brazee et al. 2011, Gilbert and Smiley 2004, Liang and Fu  
24 2012, Ostrovsky et al. 2017).

25  
26 After selecting specific colors, the boundaries of visible features in segmented images were traced to  
27 determine the intrinsic coordinates for the perimeter of the solid and damaged parts (Figure 2A–B).  
28 These sets were converted from intrinsic to Cartesian coordinates using the associated reference

1 object. Each set consisted of  $n$  clockwise-ordered coordinate pairs  $(x_i, y_i)$ ,  $\{i \mid \in 1 \dots n\}$ , that  
 2 collectively described a simple, closed curve enclosing a solid or damaged part.

3

4 *Numerical estimates*

5 Consistent with existing methods (Smiley et al. 2011), damaged wood parts were considered hollow,  
 6 or missing, for the purposes of these calculations. Four parameters were computed for the individual  
 7 shape(s) comprising each section, including the area,  $A$  ( $\text{m}^2$ ):

8 
$$A = \int dA; \quad \text{Eq. 7}$$

9 the first moment of area with respect to the y-axis,  $A_x$  ( $\text{m}^3$ ):

10 
$$A_x = \int x dA \quad \text{Eq. 8}$$

11 the first moment of area with respect to the x-axis,  $A_y$  ( $\text{m}^3$ ):

12 
$$A_y = \int y dA; \quad \text{Eq. 9}$$

13 and the second moment of area with respect to the x-axis,  $I_{xx}$  ( $\text{m}^4$ ), as in Eq. 1:

14 
$$I_{xx} = \int y^2 dA. \quad \text{Eq. 10}$$

15 Green's Theorem was used to reduce the formulas to a curve integral over the clockwise-ordered  
 16 boundary coordinates enclosing each shape. See Steger (1996) for the complete derivation of the  
 17 corresponding numerical formulas. Specifically,  $A$  was computed as:

18 
$$A = 1/2 \sum_{i=1}^n (x_i y_{i+1} - x_{i+1} y_i), \quad \text{Eq. 11}$$

19 where  $(x_i, y_i)$ ,  $\{i \mid \in 1 \dots n\}$ , are the coordinate pairs for a given shape;  $A_x$  was computed as:

20 
$$A_x = 1/6 \sum_{i=1}^n (x_i + x_{i+1})(x_i y_{i+1} - x_{i+1} y_i); \quad \text{Eq. 12}$$

21  $A_y$  was computed as:

22 
$$A_y = 1/6 \sum_{i=1}^n (y_i + y_{i+1})(x_i y_{i+1} - x_{i+1} y_i); \quad \text{Eq. 13}$$

23 and  $I_{xx}$  was computed as:

24 
$$I_{xx} = 1/12 \sum_{i=1}^n (y_i^2 + y_i y_{i+1} + y_{i+1}^2)(x_i y_{i+1} - x_{i+1} y_i). \quad \text{Eq. 14}$$

25 For small strains, the location of the neutral axis coincides with the shape's centroidal axis,  $\bar{y}$  (m),  
 26 given by:

27 
$$\bar{y} = A_y/A. \quad \text{Eq. 15}$$



1 The corresponding x-coordinate of each shape's centroid was similarly determined as:

$$2 \quad \bar{x} = A_x/A. \quad \text{Eq. 16}$$

3 For composite sections consisting of  $n$  smaller solid and hollow shapes, the centroid was determined  
4 as:

$$5 \quad \bar{y} = \sum_{j=1}^n A_{y_j} / \sum_{j=1}^n A_j, \quad \text{Eq. 17}$$

6 where  $A_{y_j}$  and  $A_j$  were multiplied by -1 if the  $j$ th shape represented a void. Similarly, the parallel axis  
7 theorem was used to determine  $I_{xx}$  for composite sections as:

$$8 \quad I_{xx} = \sum_{j=1}^n (I_{xx_j} + A_j c_j^2), \quad \text{Eq. 18}$$

9 where  $c_j$  is the perpendicular distance between the neutral axis of the composite section and the  
10 centroid of the  $j$ th smaller shape. Similarly,  $I_{xx_j}$  and  $A_j$  were multiplied by -1 if the  $j$ th shape  
11 represented a void. Ultimately,  $Z$  was computed as:

$$12 \quad Z = I_{xx}/y, \quad \text{Eq. 19}$$

13 where  $y$  is the maximum perpendicular distance between the section's neutral axis and outermost  
14 trunk fibers. The reduction to  $Z$  for a hollow section, relative to a solid section with identical trunk  
15 geometry, was determined as a percent difference:

$$16 \quad Z_{LOSS} = (Z_{SOLID} - Z_{HOLLOW})/Z_{SOLID}. \quad \text{Eq. 20}$$

17 After calculation, the estimates obtained for a given orientation were stored, and the analysis was  
18 repeated after incrementally rotating each set of coordinate pairs about the respective section's  
19 centroidal coordinates by an arbitrarily small angle. Each coordinate pair was rotated counter-  
20 clockwise about the z-axis using the following rotation matrix:

$$21 \quad R_z(\alpha) = \begin{bmatrix} \cos \alpha & -\sin \alpha \\ \sin \alpha & \cos \alpha \end{bmatrix}, \quad \text{Eq. 21}$$

22 where  $\alpha$  (rad) is the incremental rotation angle. The complete rotation for each coordinate pair was  
23 achieved by the following matrix operation:

$$24 \quad \mathbf{A}' = R_x(\alpha)(\mathbf{A} - \mathbf{B}) + \mathbf{B}, \quad \text{Eq. 22}$$

25 where  $\mathbf{A}$  is a vector in  $\mathbb{R}^2$  with elements  $[x_i \ y_i]$  and  $\mathbf{B}$  is a similar vector composed of a given section's  
26 centroidal coordinates. After each incremental rotation, identical calculations were performed to  
27 compute  $Z_{LOSS}$  until the cumulative total rotation for a section equaled  $2\pi$  rad. The preceding image

1 processing and numerical analysis steps were written as a MATLAB (MathWorks, Natick, MA, USA)  
2 function named *zloss* (Burcham 2017).

3

4 In addition, several attributes of the solid and damaged parts displayed in tomograms and binary  
5 images were calculated. The percent of total damaged cross-sectional area,  $A_D$  (%), was computed as:

$$6 \quad A_D = \frac{\sum_{i=1}^n a_{D_i}}{A_S}, \quad \text{Eq. 23}$$

7 where  $a_D$  is the area ( $\text{m}^2$ ) of  $i$ th damaged part and  $A_S$  is the area ( $\text{m}^2$ ) enclosed by the trunk boundary,  
8 excluding the bark. The offset length,  $L_O$  (m), between the centroid of the trunk and the centroid of the  
9 largest damaged part was determined using the distance formula:

$$10 \quad L_O = \sqrt{(x_2 - x_1)^2 + (y_2 - y_1)^2}, \quad \text{Eq. 24}$$

11 where  $(x_1, y_1)$  and  $(x_2, y_2)$ , respectively, are the centroidal coordinates of the trunk and largest  
12 damaged part determined numerically using Eqs. 15 and 16. The roundness,  $R$  (dimensionless), of the  
13 trunk,  $R_T$ , and largest damaged part,  $R_D$ , was determined using:

$$14 \quad R = \frac{4A}{\pi L^2}, \quad \text{Eq. 25}$$

15 where  $A$  is the area ( $\text{m}^2$ ), determined numerically using Eq. 11, and  $L$  (m) is the major axis of the  
16 shape, determined as the maximum distance between any two points on the boundary. The latter two  
17 attributes only considered the largest damaged part because existing analytical methods only  
18 explicitly consider one damaged area (Ciftci et al. 2014, Coder 1989, Smiley and Fraedrich 1992,  
19 Wagener 1963).

20

### 21 *Analytical estimates*

22 To compute analytical estimates of  $Z_{LOSS}$ , two basic approaches described by Ciftci et al. (2014) were  
23 used to approximate irregular shapes as circles. Again, only the circular approximation of the largest  
24 damaged part in a tomogram was used in the associated  $Z_{LOSS}$  calculations. For the first method  
25 (“Ciftci I”), the irregularly shaped trunk and largest damaged part were approximated using a  
26 minimum circumscribed circle, “Ciftci I(a);” maximum inscribed circle, “Ciftci I(b);” and the average  
27 of these two circles, “Ciftci I(c)”. The radius and centroidal coordinates of the minimum

1 circumscribed and maximum inscribed circles were determined using the MATLAB functions  
2 *minboundcircle* and *incircle*, respectively, from the *matGeom* library (Legland 2015). For the second  
3 method (“Ciftci II”), the radius of the circular equivalent of an irregular shape was calculated as:

$$4 \quad r = \sqrt{A/\pi}, \quad \text{Eq. 26}$$

5 where  $A$  ( $\text{m}^2$ ) is the area of an irregular shape determined numerically using Eq. 11. To position the  
6 circular equivalent shape on the centroid of its irregular counterpart, the centroidal coordinates of the  
7 trunk and largest damaged part were determined numerically using Eqs. 15 and 16. The analytical  
8 estimates of  $Z_{LOSS}$  were determined using these radii and centroidal coordinates; see Ciftci et al.  
9 (2014) for more information about the associated calculations. Since  $I_{LOSS} = Z_{LOSS}$  for a hollow circle,  
10 Eq. 2 was used, as employed by Coder (1989), to compute analytical estimates of  $Z_{LOSS}$ . Likewise, Eq.  
11 3 proposed by Wagener (1963) was used to compute analytical estimates, not strictly  $Z_{LOSS}$ , for  
12 comparison with other available methods. For Eqs. 2 (“Coder”) and 3 (“Wagener”), the radius of the  
13 circular equivalent of an irregular shape, determined using Eq. 26, was used to calculate  $Z_{LOSS}$ .

14

#### 15 *Statistical analysis*

16 Three coefficients were computed to examine the accuracy of tomograms at depicting internal  
17 conditions, in terms of the size, position, and shape of damaged parts. Pearson’s product-moment  
18 correlation ( $r$ ) and Spearman’s rank-order correlation ( $\rho$ ) were computed to measure the strength of a  
19 general linear relationship of the form  $y = ax + b$  between features estimated from tomograms and  
20 destructive measurements, including  $A_D$ ,  $L_O$ ,  $R_T$ ,  $R_D$ , and their rank-order counterparts. Lin’s  
21 concordance coefficient ( $p_c$ ) was computed to measure the strength of a linear relationship of the form  
22  $y = x$  (i.e., 1:1 similarity) between the same datasets. Cook’s D, measured during regression, was used  
23 to identify potential outliers in each comparison, with cases exerting influence greater than  $4/n$   
24 inspected more closely (Marasinghe and Kennedy 2008).

25

26 In addition, two linear models were fit to the error associated with various approaches to estimating  
27  $Z_{LOSS}$  from sonic tomograms relative to the same computed numerically from binary images. Since

1  $Z_{LOSS}$  computed numerically from binary images was based on destructive measurements and  
2 accommodated the most geometric detail, it was assumed that it provided the best available  
3 approximation of the actual  $Z_{LOSS}$  for a measured section and offered a useful standard to distinguish  
4 among other methods based on SoT. First, analysis of variance (ANOVA) was used to test the effect  
5 of the mathematical methods and colors used to select damaged wood parts on the absolute difference  
6 (%) between maximum  $Z_{LOSS}$  determined using sonic tomograms and binary images. The fixed effects  
7 included mathematical methods used to estimate  $Z_{LOSS}$ : Ciftci I(a), Ciftci I(b), Ciftci I(c), Ciftci II,  
8 Coder,  $z_{LOSS}$ , and Wagener; colors used to select damaged wood parts in sonic tomograms: violet and  
9 blue (VB) and green, violet, and blue (GVB); and their interaction: methods  $\times$  colors. For significant  
10 fixed effects, mean separation was performed using Tukey's honestly significant difference.

11

12 Second, analysis of covariance was used to test the effect of the mathematical methods on the absolute  
13 difference (%) between maximum  $Z_{LOSS}$  determined using tomograms and binary images, after  
14 accounting for geometric features of cross sections. In total, eight covariates were tested for inclusion  
15 in the model:  $A_D$ ,  $A_D(\text{error})$ ,  $L_O$ ,  $L_O(\text{error})$ ,  $R_T$ ,  $R_T(\text{error})$ ,  $R_D$ , and  $R_D(\text{error})$ . The covariates were  
16 computed from binary images of each section as described in Eqs. 23–26, and the error associated  
17 with each covariate was determined as the absolute difference between the estimate from tomograms  
18 and binary images. Since  $A_D$  represented the percent of total damaged area, the fixed effect for colors  
19 was removed from this model. The form of the model was determined by iteratively testing the  
20 significance of a simple linear relationship between each covariate and the absolute difference (%)  
21 between maximum  $Z_{LOSS}$  determined using tomograms and binary images. The validity of statistical  
22 assumptions for linear regression was checked by testing the normality of observations and  
23 homoscedasticity, respectively, with the Kolmogorov-Smirnov statistic and the Spearman rank  
24 correlation between absolute studentized residuals and observations of the dependent variable (Kutner  
25 et al. 2004). For each of the selected covariates, the homogeneity of slopes among levels of the fixed  
26 effect was tested and, if rejected, an unequal slopes model was fit for the associated covariate. For  
27 significant fixed effects, mean separation was performed using Tukey's honestly significant  
28 difference at multiple values of each covariate. Statistical analyses were performed using SAS 9.4

1 (SAS Institute, Inc., Cary, NC, USA); the ANOVA and ANCOVA models were fit using proc glm,  
2 and  $p_c$  was computed using the CCC macro v9 (Crawford et al. 2007).

### 4 **Results**

5  $A_D$ , the percent of total damaged cross-sectional area measured in sonic tomograms, was mostly less  
6 than binary images, but the difference was smaller when using GVB to select damaged parts in  
7 tomograms. On average,  $A_D$  measured in tomograms was 25% and 14%, respectively, less than binary  
8 images when using VB or GVB to select damaged parts. Significant correlations between  $A_D$   
9 measured in tomograms and binary images indicated that the size of damaged parts in tomograms was  
10 proportional to their actual size in binary images, but the difference in  $p_c$  showed that  $A_D$  computed  
11 using GVB was closer to the actual  $A_D$  in binary images (Table 2). For one yellow birch (*Betula*  
12 *alleghaniensis*) section 160 cm above ground (YB04–160),  $A_D$  measured using GVB was  
13 overpredicted by 23%, and this value was a distinct outlier ( $D = 2.12$ ) because of the  
14 disproportionately large green area in the associated tomogram. Excluding this outlier, regression  
15 indicated significant linear relationships between  $A_D$  measured from tomograms and binary images  
16 using GV ( $p < 0.001$ ) and GVB ( $p < 0.001$ ) (Table 3). For these functions, coefficients of  
17 determination indicated that  $A_D$  measured from tomograms using GV ( $r^2 = 0.54$ ) and GVB ( $r^2 = 0.59$ )  
18 accounted for considerable variation in  $A_D$  measured from binary images, suggesting that the repeated  
19 underestimation of  $A_D$  in the examined cross sections was reasonably predictable (Figure 3).

20  
21 In contrast,  $L_O$  measured in sonic tomograms was mostly greater than in binary images, but the  
22 measurements differed less when using GVB to select damaged parts in tomograms. On average,  $L_O$   
23 measured in tomograms was 4.4 cm and 3.2 cm, respectively, greater than binary images when using  
24 GV or GVB to select damaged parts. Significant correlations between  $L_O$  measured in tomograms and  
25 binary images indicated that the position of damaged parts in tomograms was proportional to their  
26 actual position in binary images, but the difference in  $p_c$  showed that  $L_O$  computed using GVB was  
27 closer to the actual  $L_O$  in binary images (Table 2). For one yellow birch cross section 100 cm above  
28 ground (YB05–100),  $L_O$  measured using VB was overpredicted by 26.3 cm. This value was a distinct

1 outlier ( $D = 2.11$ ) because the largest damaged part was depicted near the trunk periphery in the  
2 tomogram – a considerable distance from the largest damaged part at the center of the cross section in  
3 the corresponding binary image. Excluding this outlier, regression indicated significant linear  
4 relationships between  $L_O$  measured from tomograms and binary images using GV ( $p < 0.001$ ) and  
5 GVB ( $p < 0.001$ ) (Table 3). For these functions, coefficients of determination indicated that  $L_O$   
6 measured from tomograms using GV ( $r^2 = 0.62$ ) and GVB ( $r^2 = 0.56$ ) accounted for considerable  
7 variation in  $L_O$  measured from binary images, suggesting that the repeated overestimation of  $L_O$  in the  
8 examined cross sections was reasonably predictable (Figure 4). For these regression functions, the  
9 intercept was not significantly different from zero when using GV ( $p = 0.736$ ) or GVB ( $p = 0.927$ ) to  
10 select damaged parts in tomograms, indicating that the overestimation of  $L_O$  in tomograms increased  
11 in proportion to the actual  $L_O$  in binary images (Figure 4).

12

13 On average,  $R_T$  for sonic tomograms (mean = 0.850) and binary images (mean = 0.841) was greater  
14 than  $R_D$  measured in binary images (mean = 0.570) and tomograms using GV (mean = 0.512) or GVB  
15 (mean = 0.570), indicating that a circle better approximated the shape of trunks than damaged parts  
16 for this set of trees. Among all geometric features examined in this study,  $r$ ,  $\rho$ , and  $p_c$  were the greatest  
17 for  $R_T$  measured in tomograms and binary images, indicating that  $R_T$  depicted in tomograms was very  
18 similar to the actual  $R_T$  in binary images (Table 2). Regression indicated a significant linear  
19 relationship between  $R_T$  measured from tomograms and binary images ( $p < 0.001$ ) with a high  
20 coefficient of determination ( $r^2 = 0.66$ ) (Table 3, Figure 5).

21

22 In contrast, the shape of damaged parts in binary images, measured in terms of  $R_D$ , was poorly  
23 depicted in sonic tomograms, and this was especially true for damaged parts selected using only VB.  
24 Among all geometric features examined in this study,  $r$ ,  $\rho$ , and  $p_c$  were the lowest for  $R_D$  measured in  
25 tomograms and binary images, implying greater dissimilarity between the  $R_D$  measured using the two  
26 images. Regression indicated a significant linear relationship only between  $R_D$  measured in  
27 tomograms and binary images using GVB ( $p < 0.001$ ); and the associated coefficients of

1 determination indicated that  $R_D$  determined using GV ( $r^2 = 0.05$ ) and GVB ( $r^2 = 0.25$ ) in tomograms  
2 accounted for little variation in  $R_D$  measured from binary images (Table 3).

3

4 Analysis of variance indicated that the mathematical methods and colors used to select damaged parts  
5 significantly affected the absolute difference (%) between  $Z_{LOSS}$  determined using tomograms and  
6 binary images, but these two factors did not interact to affect the absolute difference between  $Z_{LOSS}$   
7 determined using the two image types (Table 4). Overall, the absolute difference (%) between  $Z_{LOSS}$   
8 determined using tomograms and binary images was significantly less for estimates using GVB to  
9 select damaged parts than for others using VB. Overall, the average absolute difference in  $Z_{LOSS}$  was  
10 6% less for estimates using GVB compared to others using only VB. Among mathematical methods,  
11 pairwise comparisons revealed that the absolute difference between  $Z_{LOSS}$  determined using  
12 tomograms and binary images was significantly greater for analytical methods neglecting the position  
13 of damaged parts (i.e., Coder and Wagener). Overall, the error associated with these estimates was  
14 between 5% and 9% greater than for other methods, which did not differ significantly from one  
15 another (Table 4).

16

17 In terms of the actual difference between  $Z_{LOSS}$  determined using tomograms and binary images, all  
18 mathematical methods underestimated  $Z_{LOSS}$  in most cases. For Coder and Wagener, respectively,  
19  $Z_{LOSS}$  determined using tomograms was, on average, 25% and 21% less than determined numerically  
20 using binary images; these two methods underestimated  $Z_{LOSS}$  in 98% of all cases. For the remaining  
21 methods, the average actual difference was smaller, but the estimates determined using tomograms  
22 were still less than determined numerically using binary images in most cases. Among these methods,  
23 the average actual difference between  $Z_{LOSS}$  determined using tomograms and binary images was, in  
24 decreasing order: Ciftci I(b), 14%; Ciftci II, 11%; Ciftci I(c), 9%;  $z_{loss}$ , 9%; Ciftci I(a), 4%.

25

26 Among all tested covariates,  $L_O$  ( $F = 26.72$ ;  $df = 7, 658$ ;  $p < 0.001$ ) and  $A_D(\text{error})$  ( $F = 17.68$ ;  $df = 7,$   
27  $658$ ;  $p < 0.001$ ) were selected as the only variables showing a significant linear relationship with the  
28 absolute difference between  $Z_{LOSS}$  determined using tomograms and binary images. Although the

1 slopes describing the change in the absolute difference between  $Z_{LOSS}$  determined using tomograms  
2 and binary images over a unit change in  $L_O$  varied significantly among mathematical methods ( $F =$   
3  $4.95$ ;  $df = 6, 658$ ;  $p < 0.001$ ), the same was not true for the slopes describing the change in this  
4 difference over a unit change in  $A_D(\text{error})$  ( $F = 1.17$ ;  $df = 6, 658$ ;  $p = 0.322$ ). As a result, a common  
5 slope was used to describe the relationship between  $A_D(\text{error})$  and the absolute difference between  
6  $Z_{LOSS}$  determined using tomograms and binary images for all mathematical methods, and unequal  
7 slopes were fit to describe the relationship between  $L_O$  and the absolute difference between  $Z_{LOSS}$   
8 determined using tomograms and binary images for each mathematical method individually. Using  
9 this model, analysis of covariance revealed that mathematical methods significantly affected the  
10 absolute difference between  $Z_{LOSS}$  determined using tomograms and binary images, after accounting  
11 for  $L_O$  and  $A_D(\text{error})$ . Except for Coder, the intercepts associated with each method were not  
12 significantly different from zero, indicating that the absolute difference between  $Z_{LOSS}$  determined  
13 using tomograms and binary images is minimized to effectively zero for most mathematical methods  
14 when the largest damaged part is concentric and  $A_D$  is depicted accurately in tomograms. Except for  
15  $z_{loss}$ , all the slopes describing the relationship between  $L_O$  and the absolute difference between  $Z_{LOSS}$   
16 determined using tomograms and binary images were significantly different from zero, indicating  
17 that, among all methods, the numerical approach was the least sensitive to changes in  $L_O$  (Table 5).

18

19 Mean separation, performed at six combinations of the two covariates selected to represent the  
20 observed range of  $A_D(\text{error})$  and  $L_O$  revealed that differences among mathematical methods existed  
21 only for  $L_O > 0$ . At  $A_D(\text{error}) = 0$  and  $L_O = 0$ , there were no significant differences in the absolute  
22 difference between  $Z_{LOSS}$  determined using tomograms and binary images among mathematical  
23 methods, and there were similarly no significant differences among methods at  $A_D(\text{error}) = 0.4$  and  $L_O$   
24  $= 0$ , since a common slope was fit to all observations of  $A_D(\text{error})$  and the absolute difference between  
25  $Z_{LOSS}$  determined using tomograms and binary images. For all mathematical methods, the absolute  
26 difference between  $Z_{LOSS}$  determined using tomograms and binary images increased by 46% over a  
27 unit change in  $A_D(\text{error})$  (note that the possible range for  $A_D(\text{error})$  is  $[0, 1]$ ). However, consistent  
28 differences arose among mathematical methods for  $L_O > 0$ , owing to the different slopes fit to



1 observations of  $L_O$  and the absolute difference between  $Z_{LOSS}$  determined using tomograms and binary  
2 images for each method separately (Table 5). For these cases, the absolute difference between  $Z_{LOSS}$   
3 determined using tomograms and binary images was greatest for Coder and Wagener, since these  
4 methods neglected  $L_O$ . The remaining methods, in decreasing order of the absolute difference between  
5  $Z_{LOSS}$  determined using tomograms and binary images, were: Ciftci I(b), Ciftci II, Ciftci I(c), Ciftci  
6 I(a), and  $z_{loss}$  (Table 6).

7

## 8 **Discussion**

9 For decayed sections, most authors similarly observed that  $A_D$  was underestimated in sonic  
10 tomograms in a range of tree species (Deflorio et al. 2008, Gilbert and Smiley 2004, Liang et al. 2007,  
11 Liang and Fu 2012, Marra et al. 2018, Wang et al. 2007, Wang et al. 2009). In agreement with these  
12 findings, Wang et al. (2009) also reported that the average difference between  $A_D$  determined using  
13 sonic tomograms and destructive measurements was greater when using VB (mean = 14%) than GVB  
14 (mean = 2%) to select damaged parts. In other reports, authors only used two colors to select damaged  
15 parts in sonic tomograms, and the reported average underestimation of  $A_D$  ranged between  $< 1\%$   
16 (Ostrovsky et al. 2017) and 14% (Wang et al. 2009). However, some authors computed  $A_D$  using  
17 coarse grid systems with cell dimensions ranging between 5 mm (Gilbert and Smiley 2004) and 12.5  
18 mm (Ostrovsky et al. 2017), contributing unknown error to the approximation.

19

20 It is possible that the underestimation of  $A_D$  arises from the reduced sensitivity of sonic tomography to  
21 low velocity features (Li et al. 2012) that limits the detection of incipient decay (Deflorio et al. 2008),  
22 and practitioners should account for this limitation when interpreting tomograms, especially in light of  
23 the consensus among related studies. Others have reported, in agreement with this study, a strong  
24 linear relationship between  $A_D$  determined using tomograms and destructive measurements (Gilbert  
25 and Smiley 2004, Liang and Fu 2012). In a sample of 15 decayed sections, Liang and Fu (2012)  
26 reported much better agreement between  $A_D$  determined using sonic tomograms and destructive  
27 measurements; the slope of a linear model fit to these observations was much closer to one than in this  
28 study, with a high coefficient of determination ( $r^2 = 0.94$ ) despite using only VB to select damaged

1 parts. Although Gilbert and Smiley (2004) also reported a strong linear relationship between the  
2 amount of decay depicted in tomograms and measured on images of decayed cross sections ( $r^2 =$   
3 0.94), the authors did not fit a linear regression model to the observations, precluding a comparison of  
4 model coefficients. Compared to existing reports, there was a greater underestimation of  $A_D$  in sonic  
5 tomograms in this study. Still, practitioners should use caution when considering the use of regression  
6 models from this study to adjust tomographic estimates because the underlying observations were  
7 limited to three species at a single site. Although our sample of decayed sections was relatively large,  
8 it will be important to examine further the relationship between  $A_D$  determined using tomograms and  
9 destructive measurements across several sites and species in future work.

10

11 Conversely, most existing reports indicated that  $A_D$  was overestimated in sonic tomograms for  
12 sections with internal cracks (Liang et al. 2007, Wang et al. 2009, Wang and Allison 2008). In this  
13 study, only one of the examined sections (SM05–100) contained a crack, but it occurred alongside  
14 internal decay, preventing a separate evaluation of this type of defect. Without adjustment, this means  
15 that  $Z_{LOSS}$  determined using tomograms would tend to be liberal and conservative for cracks and  
16 decay, respectively, and practitioners should consider these trends when computing  $Z_{LOSS}$  from  
17 tomograms. Future studies should examine the accuracy of tomograms, in terms of  $A_D$ , for each type  
18 of defect separately, taking care to separate those cracks present during tomographic measurement  
19 from others created by drying after felling.

20

21 Among related studies, this is the first report of a repeated overestimation of  $L_O$  in sonic tomograms.  
22 In a sample of 17 decayed sections, Gilbert and Smiley (2004) observed that, in terms of the location  
23 of damaged parts, 2% and 9% of  $A_D$  were false-positive and -negative estimates that did not match the  
24 internal condition of sections. However,  $L_O$  is arguably a better feature to examine, in terms of  $Z_{LOSS}$ ,  
25 because damaged parts decrease  $I$  proportional to the square of this distance (Eq. 18). The observed  
26 repeated overestimation of  $L_O$  in sonic tomograms should contribute to an equivalent overestimation  
27 of  $Z_{LOSS}$ , proportional to  $A_D$  (Eq. 18). Like  $A_D$ , the difference between  $L_O$  determined using tomograms  
28 and binary images was greater when using VB than GVB to select damaged parts, further justifying

1 the addition of color(s) representing intermediate acoustic transmission speeds when analyzing  
2 tomograms, despite its usual omission by the manufacturer's software.  
3  
4 The accuracy of  $Z_{LOSS}$  estimates improved when using GVB to select damaged parts, corroborating the  
5 direct comparisons between geometric attributes in this study and other reports that these colors  
6 should be used to select damaged parts (Marra et al. 2018, Wang et al. 2009). Among the evaluated  
7 methods, the difference between  $Z_{LOSS}$  determined using tomograms and binary images for Coder and  
8 Wagener was significantly greater than all other methods. Considering this difference, practitioners  
9 should avoid using methods neglecting  $L_O$  to estimate  $Z_{LOSS}$ , in agreement with Kane and Ryan  
10 (2004). Although Liang and Fu (2012) reported a much smaller difference between strength-loss  
11 estimates determined using tomograms and destructive measurements, the reported difference was  
12 determined only by the accuracy of tomograms because the same method was applied to tomograms  
13 and destructive measurements in each case. In this study, the methods used to estimate  $Z_{LOSS}$  from  
14 tomograms were compared with an improved numerical method,  $z_{loss}$ , applied to binary images.  
15  
16 The difference between  $Z_{LOSS}$  determined using tomograms and binary images did not vary with  $R_T$  or  
17  $R_D$ , supporting the use of circles to approximate irregular shapes by existing analytical methods  
18 (Ciftci et al. 2014, Coder 1989, Smiley and Fraedrich 1992, Wagener 1963). However, some authors  
19 have reported that  $A_D(\text{error}) \propto R^{-1}$  (Gilbert et al. 2016, Rabe et al. 2004, Rust 2017), and the use of  
20 circles for highly irregular trunk shapes may be less appropriate in these situations. The selection of  
21  $A_D(\text{error})$  and  $L_O$  as covariates means that the accuracy of  $Z_{LOSS}$  estimates was primarily affected by  
22 the underestimation of  $A_D$  in tomograms and the actual  $L_O$  of the largest damaged part. Based on this  
23 analysis, it is apparent that the value of a method, relative to others examined in this study, depends  
24 largely on its consideration and approach to  $L_O$ ; all methods were similarly affected by the  
25 underestimation of  $A_D$  in sonic tomograms. After accounting for  $A_D(\text{error})$  and  $L_O$ , the consistent  
26 ranking among methods used to estimate  $Z_{LOSS}$ , caused by the unequal slopes fit to each method for  
27  $L_O$ , usefully revealed methods that should be considered for greater use by arborists. Uniquely, the  
28 slope fit to  $z_{loss}$  was not significantly different from zero, and the absolute difference between  $Z_{LOSS}$

1 determined using tomograms and binary images was lowest for this method at all selected values of  
2 the covariates. As a result, the accuracy of this method was mostly determined by the error in  
3 estimating  $A_D$ , and this provides justification for using this method as a benchmark, since it was least  
4 sensitive to changes in  $L_O$ .

5  
6 Among the remaining analytical methods proposed by Ciftci et al. (2014), Ciftci I(a) and I(c) gave  
7 better estimates, in terms of the absolute difference between  $Z_{LOSS}$  determined using tomograms and  
8 binary images, than Ciftci II and I(b). The former two methods relied, in whole or part, on  
9 circumscribed circles fit to the trunk and largest damaged part. Since  $R_T > R_D$  for the examined  
10 sections, the circumscribed circles enlarged the area of damaged parts (mean: +86%) more than trunks  
11 (mean: +19%), relative to their corresponding area in tomograms, resulting in an average increase to  
12  $A_D$  of 7.5% and 2.5%, respectively, for Ciftci I(a) and I(c). The increased  $A_D$  usefully offset its  
13 underestimation in tomograms, explaining the improved estimates offered by these two methods.  
14 Notably, solutions were available in all cases using Ciftci I(a), but the same was not true for all cases  
15 using other methods. For example,  $Z_{LOSS}$  could not be estimated using Ciftci I(b), I(c), and II for one  
16 sugar maple cross section 80 cm above ground (SM28–080) because the damaged part was  
17 completely outside and did not intersect the solid trunk. Although Ciftci I(a) offered relatively  
18 superior estimates among analytical methods proposed by Ciftci et al. (2014), it is useful to note that  
19 these methods are not strictly analytical because they require image processing techniques, limiting  
20 their usefulness to practitioners.

21  
22 Despite considering only the largest damaged part, the analytical estimates differed modestly from the  
23 numerical estimate computed from binary images in most cases. On average, the percent of total area  
24 occupied by the largest damaged part was 11% (SD 16%) less than  $A_D$ . Still, the analytical methods  
25 gave sizeable underestimates of  $Z_{LOSS}$  in some cases because they neglected to consider one or more  
26 additional damaged parts. In one American beech section 60 cm above ground (AB06–060), the  
27 largest damaged part was in the center of the section, but the analytical estimate omitted the

1 contributions from the second largest damaged part at the trunk periphery, causing  $Z_{LOSS}$  to be  
2 underestimated by, on average, 16% among the six analytical methods.

3  
4 The PiCUS Q74 software, like other sonic tomography devices, provides a built-in function to give an  
5 approximate estimate of the percent residual load-bearing capacity (Gocke 2017) equal to:

$$6 \quad I_{du}/I_{Du} \times 100, \quad \text{Eq. 27}$$

7 where  $I_{du}$  and  $I_{Du}$  are the second moments of area computed about the section's centroid using the  
8 diameter of the damaged part ( $d$ ) and trunk ( $D$ ). To determine these diameters, the software requires  
9 users to select the boundary between damaged and solid wood, and it computes the lengths along a  
10 radius formed by the centroid and user-selected location (A. Richter, personal communication). This  
11 excludes considerable information in the tomogram from the estimate. Since Eq. 27 corresponds to 1  
12 – Eq. 2, its performance can be considered equivalent to that ascribed to Coder in this study.

13 Practitioners are cautioned against using this built-in function when eccentric decay is present because  
14 Kane and Ryan (2004) demonstrated that Eq. 2 performed poorly in these cases.

15  
16 It is possible that the image binarization process used in this study introduced unknown error into the  
17  $Z_{LOSS}$  estimates derived from binary images. Although the existence of damaged wood was obvious in  
18 most of the examined sections, error may have occurred in determining the precise boundary between  
19 damaged and solid wood. In the future, authors should consider alternative methods to binarize  
20 images for  $Z_{LOSS}$  estimates. Likewise, the assumption of material isotropy may have introduced  
21 negligible error into the  $Z_{LOSS}$  estimates (Ciftci et al. 2014), and authors should consider these effects,  
22 when relevant material properties information is available, in future work.

## 23 24 **Conclusion**

25 Among the evaluated methods,  $Z_{LOSS}$  was best estimated using sonic tomograms numerically with  
26  $z_{loss}$  or analytically with Ciftci I(a), and practitioners should consider using these methods to assess  
27 the severity of internal defects measured with sonic tomography. The numerical method  $z_{loss}$   
28 addressed the simplifying assumptions contained in many existing methods by accommodating more

1 geometric detail in the associated calculations, including irregular shapes and multiple offset damaged  
2 parts. Still, the repeated under- and overestimation, respectively, of  $A_D$  and  $L_O$  in tomograms limits the  
3 accuracy of  $Z_{LOSS}$  estimates based on tomography, and these limitations should be considered when  
4 interpreting estimates. It is important to note that  $Z_{LOSS}$  only estimates the reduced load-bearing  
5 capacity of the measured tree part (not the entire tree). Even more, the methods described in this  
6 article do not estimate the probability of tree failure, which requires a more thorough accounting of  
7 the total applied and resistive forces acting on a tree. There is little scientific consensus on a threshold  
8 value associated with a change in the likelihood of failure (Gruber 2008), but Kane (2014) showed  
9 that failure at an area with existing or simulated decay was more likely when  $I_{LOSS} > 30\%$ .

10

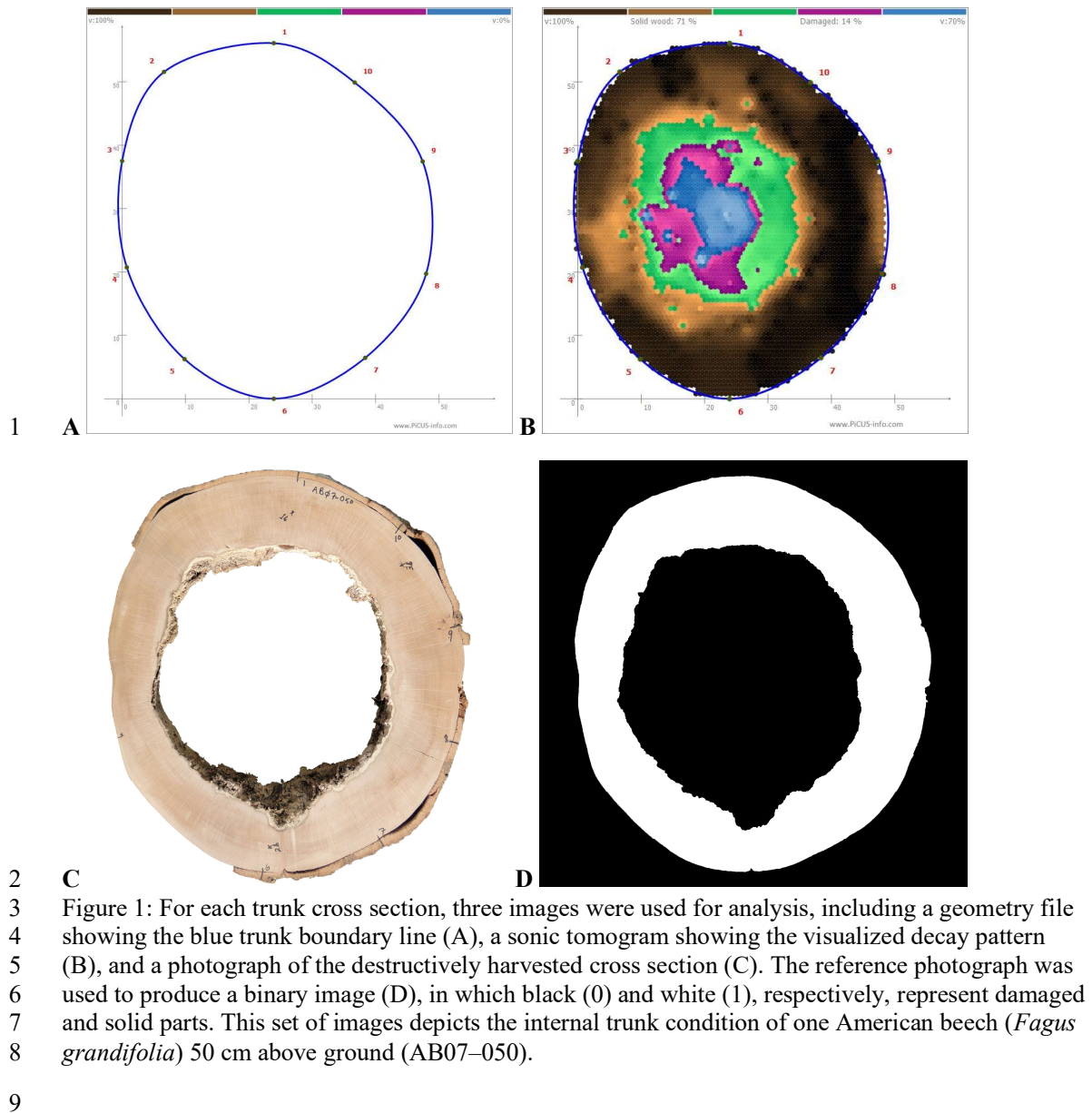
#### 11 **Literature cited**

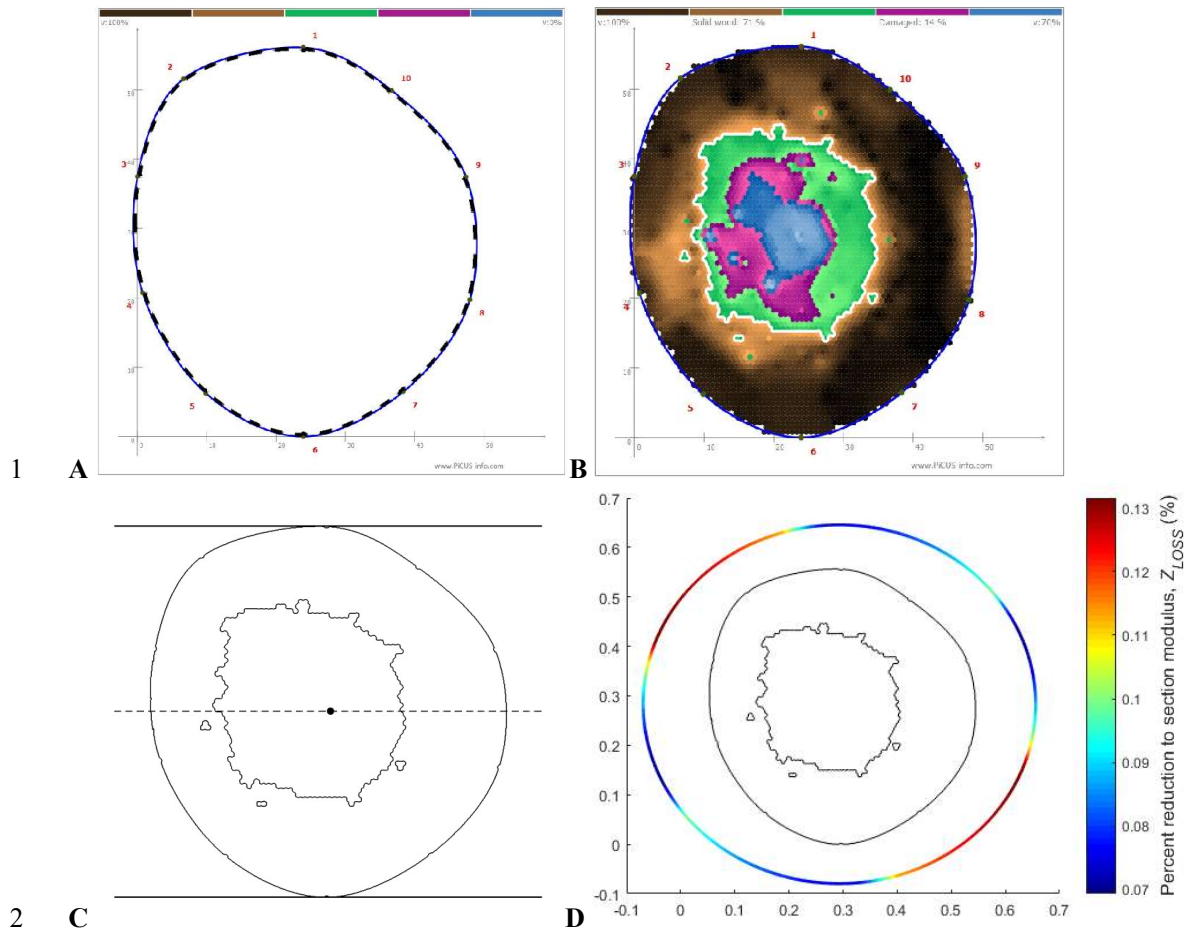
- 12 Arciniegas A, Prieto F, Brancheriau L, Lasaygues P (2014) Literature review of acoustic and  
13 ultrasonic tomography in standing trees. *Trees* 28:1559-1567
- 14 Brazee NJ, Marra RE, Gocke L, Van Wassenae P (2011) Non-destructive assessment of internal  
15 decay in three hardwood species of northeastern North America using sonic and electrical  
16 impedance tomography. *Forestry* 84:33-39
- 17 Burcham DC (2017) *zloss*. GitHub, version 1.1 <https://github.com/danielburcham/zloss>
- 18 Ciftci C, Kane B, Brena SF, Arwade SR (2014) Loss in moment capacity of tree stems induced by  
19 decay. *Trees* 28:517-529
- 20 Coder KD (1989) Should or shouldn't you fill tree hollows?. *Grounds Maint* 24:68-70, 72-73, 100
- 21 Crawford SB, Kosinski AS, Lin HM, Williamson JM, Barnhart HX (2007) Computer programs for  
22 the concordance correlation coefficient. *Comput Methods Programs Biomed* 88:62-74
- 23 Deflorio G, Fink S, Schwarze FW (2008) Detection of incipient decay in tree stems with sonic  
24 tomography after wounding and fungal inoculation. *Wood Sci Technol* 42:117-132
- 25 Ennos AR (2012) *Solid Biomechanics*. Princeton University Press, Princeton, NJ, USA
- 26 Gilbert EA, Smiley ET (2004) Picus sonic tomography for the quantification of decay in white oak  
27 (*Quercus alba*) and hickory (*Carya* spp.). *J Arboric* 30:277-281
- 28 Gilbert GS, Ballesteros JO, Barrios-Rodriguez CA, Bonadies EF, Cedeno-Sanchez ML, Fossatti-  
29 Caballero NJ, Trejos-Rodriguez MM, Perez-Suniga JM, Holub-Young KS, Henn LAW,  
30 Thompson JB, Garcia-Lopez CG, Romo AC, Johnston DC, Barrick PP, Jordan FA, Hershovich  
31 S, Russo N, Sanchez JD, Fabrega JP, Lumpkin R, McWilliams HA, Chester KN, Burgos AC,  
32 Wong EB, Diab JH, Renteria SA, Harrower JT, Hooton DA, Glenn TC, Faircloth BC, Hubbell  
33 SP (2016) Use of sonic tomography to detect and quantify wood decay in living trees. *Appl Plant*  
34 *Sci* 4:1-13

- 1 Gocke L (2017) PiCUS Sonic Tomograph: Software Manual Q74:1-92
- 2 Gruber F (2008) Reply to the response of Claus Mattheck and Klaus Bethge to my criticisms on  
3 untenable VTA-failure criteria. Who is right and who is wrong?. *Arboric J* 31:277-296
- 4 Johnstone D, Moore G, Tausz M, Nicolas M (2010) The measurement of wood decay in landscape  
5 trees. *Arboric Urban For* 36:121-127
- 6 Kane B (2014) Determining parameters related to the likelihood of failure of red oak (*Quercus rubra*  
7 L.) from winching tests. *Trees* 28:1667-1677
- 8 Kane B, Ryan HDP (2004) The accuracy of formulas used to assess strength loss due to decay in  
9 trees. *J Arboric* 30:347-356
- 10 Kane B, Ryan HDP, Bloniarz DV (2001) Comparing formulae that assess strength loss due to decay  
11 in trees. *J Arboric* 27:78-87
- 12 Koizumi A, Hirai T (2006) Evaluation of the section modulus for tree-stem cross sections of irregular  
13 shape. *J Wood Sci* 52:213-219
- 14 Kutner MH, Nachtsheim CJ, Neter J (2004) *Applied Linear Regression Models*. McGraw-Hill Irwin,  
15 Boston, MA, USA
- 16 Legland D (2015) *matGeom*. GitHub, <https://github.com/mattools/matGeom/>
- 17 Li L, Wang X, Wang L, Allison RB (2012) Acoustic tomography in relation to 2D ultrasonic velocity  
18 and hardness mappings. *Wood Sci Technol* 46:551-561
- 19 Liang S, Fu F (2012) Strength loss and hazard assessment of Euphrates poplar using stress wave  
20 tomography. *Wood Fiber Sci* 44:1-9
- 21 Liang S, Wang X, Wiedenbeck J, Cai Z, Fu F (2007) Evaluation of acoustic tomography for tree  
22 decay detection. 15th International Symposium on Nondestructive Testing of Wood Duluth, MN,  
23 USA, pp 49-54
- 24 Marasinghe MG, Kennedy WJ (2008) SAS for Data Analysis: Intermediate Statistical Methods. In:  
25 Chambers J, Hardle W, Hand D (eds) *Statistics and Computing*. Springer, New York, NY, USA,  
26 pp 557
- 27 Marra RE, Brazeel N, Fraver S (2018) Estimating carbon loss due to internal decay in living trees  
28 using tomography: implications for forest carbon budgets. *Environ Res Lett* 13:105004
- 29 Niklas KJ (1992) *Plant Biomechanics: An Engineering Approach to Plant Form and Function*.  
30 University of Chicago Press, Chicago, IL, USA
- 31 Ostrovsky R, Kobza M, Gazo J (2017) Extensively damaged trees tested with acoustic tomography  
32 considering tree stability in urban greenery. *Trees* 31:1015-1023
- 33 Rabe C, Ferner D, Fink S, Schwarze FW (2004) Detection of decay in trees with stress waves and  
34 interpretation of acoustic tomograms. *Arboric J* 28:3-19
- 35 Rust S (2017) Accuracy and reproducibility of acoustic tomography significantly increase with  
36 precision of sensor position. *J Forest Landscape Res* 1:1-6

- 1 Smiley ET, Matheny N, Lilly S (2011) Tree Risk Assessment. International Society of Arboriculture,  
2 Champaign, IL, USA
- 3 Smiley ET, Fraedrich BR (1992) Determining strength loss from decay. *J Arboric* 18:201-204
- 4 Steger C (1996) On the calculation of moments of polygons. Munich, Germany, Technical University  
5 of Munich, FGBV-96-04, pp 1-14
- 6 Wagener WW (1963) Judging Hazard from Native Trees in California Recreational Areas: A Guide  
7 for Professional Foresters. Berkeley, CA, USA, Pacific Southwest Forest and Range Experiment  
8 Station, Forest Service, US Department of Agriculture, PSW-P1, pp 1-29
- 9 Wang X, Wiedenbeck J, Liang S (2009) Acoustic tomography for decay detection in black cherry  
10 trees. *Wood Fiber Sci* 41:127-137
- 11 Wang X, Allison RB, Wang L, Ross RJ (2007) Acoustic tomography for decay detection in red oak  
12 trees. Madison, WI, USA, Forest Products Laboratory, Forest Service, US Department of  
13 Agriculture, FPL-RP-642, pp 1-7
- 14 Wang X, Allison RB (2008) Decay detection in red oak trees using a combination of visual  
15 inspection, acoustic testing, and resistance microdrilling. *Arboric Urban For* 34:1-4
- 16

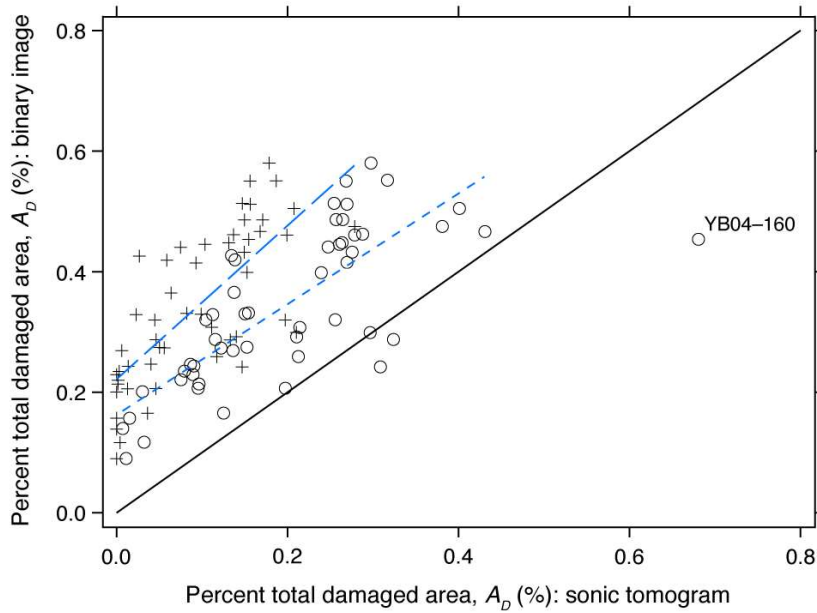






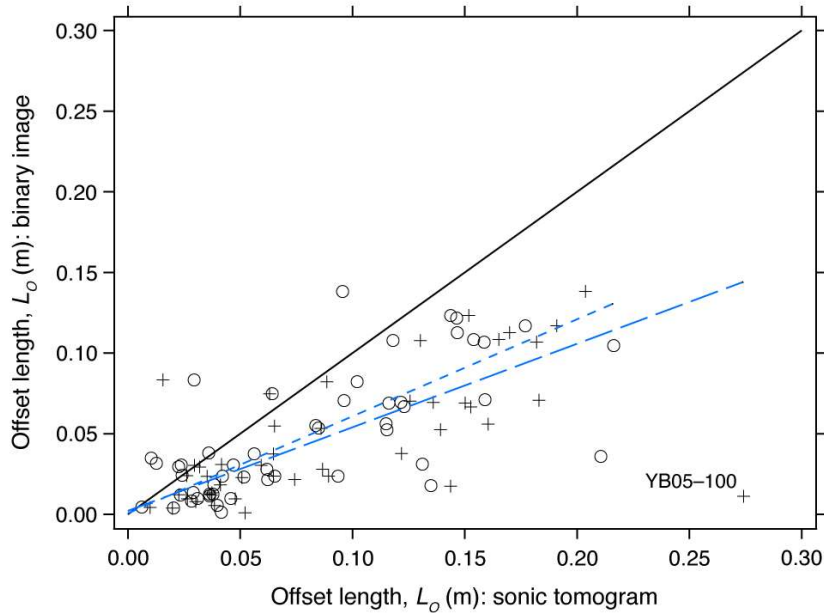
2 **C**  
 3 Figure 2: Using specific ranges in the HSV and LAB color space, respectively, sonic tomograms were  
 4 segmented to acquire the boundary of solid (A: dashed black line) and damaged (B: solid white lines)  
 5 parts. For a given orientation, the perimeters of shapes comprising each hollow section were used to  
 6 determine several features, including the neutral axis (C: dashed horizontal line), centroid (C: solid  
 7 dot), and the outermost trunk fibers oriented perpendicular to the neutral axis (C: solid horizontal  
 8 lines). The  $Z_{LOSS}$  estimates are displayed as color intensity values on a circular annulus surrounding an  
 9 outline of each hollow section (D). The red, green, blue continuous color scale represents directional  
 10  $Z_{LOSS}$  between the minimum and maximum value for a given cross section.

11



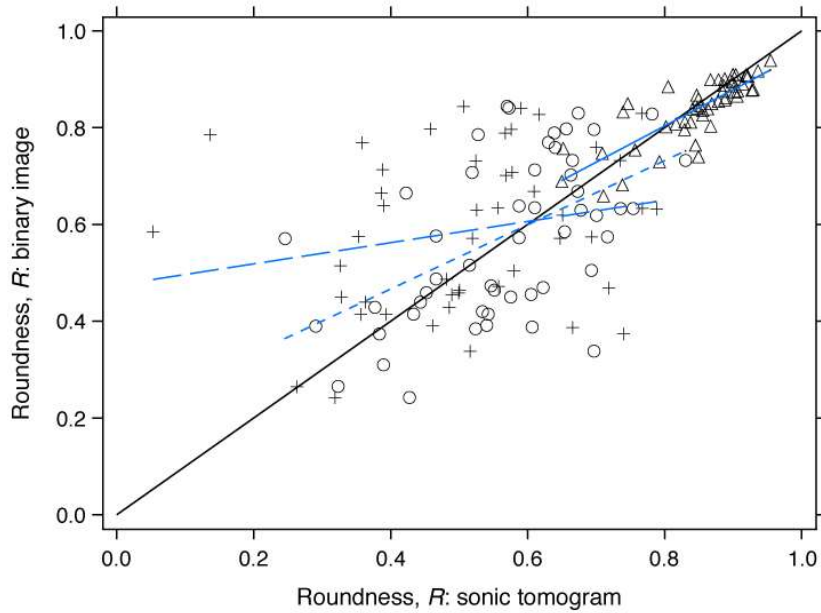
1  
2  
3  
4  
5  
6  
7  
8  
9  
10  
11  
12

Figure 3: Scatter plot of the percent of total damaged cross-sectional area,  $A_D$  (%), measured in sonic tomograms against  $A_D$  measured in a reference binary image of the destructively measured internal condition of trees. For the estimates derived from tomograms, damaged parts were selected using either green, violet, and blue (GVB, circle) or violet and blue (VB, plus). Most values are located above the solid black 1:1 comparison line, indicating a repeated underestimation of  $A_D$  in tomograms relative to binary images. In contrast,  $A_D$  measured using GVB for one yellow birch (*Betula alleghaniensis*) trunk 160 cm above ground (labeled YB04-160) was overpredicted by 23%, a distinct outlier. Least squares regression equations are  $y = 0.22 + 1.27x$  (blue, long dash line) and  $y = 0.16 + 0.92x$  (blue, short dash line) for  $A_D$  computed using VB and GVB, respectively. See Table 3 for model parameter estimates and fit statistics.



1  
2 Figure 4: Scatter plot of the offset length,  $L_o$  (m), measured in sonic tomograms against  $L_o$  measured  
3 in a reference binary image of the destructively measured internal condition of trees. For the estimates  
4 derived from tomograms, damaged parts were selected using either green, violet, and blue (GVB,  
5 circle) or violet and blue (VB, plus). Most values are located below the solid black 1:1 comparison  
6 line, indicating a repeated overestimation of  $L_o$  in tomograms relative to binary images. Uniquely,  $L_o$   
7 measured using two colors for one yellow birch (*Betula alleghaniensis*) trunk 100 cm above ground  
8 (labeled YB05–100) was overpredicted by 26.3 cm, a distinct outlier. Least squares regression  
9 equations are  $y = 6.59 \times 10^{-4} + 0.60x$  (blue, long dash line) and  $y = 2.18 \times 10^{-3} + 0.52x$  (blue, short dash  
10 line) for  $L_o$  computed using VB and GVB, respectively. See Table 3 for model parameter estimates  
11 and fit statistics.

12



1

2 Figure 5: Scatter plot of the roundness,  $R$  (dimensionless), of the largest damaged part,  $R_D$ , and trunk,  
 3  $R_T$ , measured in sonic tomograms against the same measured in a binary image of the destructively  
 4 measured internal condition of trees. For the estimates derived from tomograms,  $R_D$  was determined  
 5 using either green, violet, and blue (GVB, circle) or violet and blue (VB, plus);  $R_T$  was computed  
 6 using the blue trunk geometry line (triangle). Least squares regression equations are  $y = 0.47 + 0.22x$   
 7 (blue, long dash line) and  $y = 0.20 + 0.75x$  (blue, short dash line) for  $R_D$  computed using VB and  
 8 GVB, respectively; the equation for  $R_T$  is  $y = 0.20 + 0.75x$  (blue, solid line). See Table 3 for model  
 9 parameter estimates and fit statistics.

10

1 Table 1: Histogram thresholds used to select specific ranges in the HSV and LAB color space,  
 2 respectively, associated with solid and damaged parts in sonic tomograms

	<b>Geometry</b>	<b>Sonic tomogram</b>	
<b>Color(s)</b>	Blue	Green, violet, blue (GVB) <sup>a</sup>	Violet, blue (VB)
<b>Color Space</b>	HSV	LAB	LAB
<b>Component 1</b>	[0.01, 0.78] <sup>b</sup>	[20.92, 100.00]	[0.00, 100.00]
<b>Component 2</b>	[0.16, 1.00]	[-26.90, 81.98]	[-68.60, -10.46]
<b>Component 3</b>	[0.00, 1.00]	[-63.54, -3.78]	[-99.92, 62.94]

3 <sup>a</sup>For each sonic tomogram, either violet and blue (VB) or green, violet, and blue (GVB) was used to  
 4 select damaged parts. In a PiCUS® sonic tomogram, the four colors used to visualize sonic velocities  
 5 and the corresponding internal wood condition are as follows: brown, solid; green, intermediate;  
 6 violet, damaged; and blue, damaged.

7 <sup>b</sup>The ranges for each color component are expressed using interval notation.

8

1 Table 2: For a set of 51 trunk cross sections, Pearson's product-moment correlation ( $r$ ), Spearman's  
 2 rank-order correlation ( $\rho$ ), and Lin's concordance correlation ( $p_c$ ) between geometric attributes  
 3 derived from sonic tomograms and binary images of the destructively measured internal condition of  
 4 trees.

$A_D$ (%)	$r$	$\rho$	$p_c$
VB <sup>b</sup>	0.74**	0.80**	0.16
GVB	0.71**	0.77**	0.44
<b><math>L_O</math> (m)</b>			
VB	0.64**	0.64**	0.41
GVB	0.70**	0.68**	0.53
<b><math>R_T</math></b>			
-	0.82**	0.83**	0.81
<b><math>R_D</math></b>			
VB	0.22	0.26	0.20
GVB	0.55**	0.54**	0.53

5 Geometric attributes include  $A_D$  (%), the percent of total damaged cross-sectional area;  $L_O$  (m), the  
 6 offset length between the centroid of the trunk and the centroid of the largest damaged part; and  $R$   
 7 (dimensionless), the roundness of the trunk,  $R_T$ , and largest damaged part,  $R_D$ .

8 <sup>b</sup>For each sonic tomogram, either violet and blue (VB) or green, violet, and blue (GVB) was used to  
 9 select damaged parts. In a PiCUS® sonic tomogram, the four colors used to visualize acoustic  
 10 transmission speeds and the corresponding internal wood condition are as follows: brown, solid;  
 11 green, intermediate; violet, damaged; and blue, damaged.

12

1 Table 3: Parameter estimates, confidence intervals, and coefficients of determination for linear  
 2 regression models fit to geometric attributes derived from sonic tomograms and binary images of the  
 3 destructively measured internal condition of trees.

$A_D$ (%)	$b$ (95% CI)	$p$	$a$ (95% CI)	$p$	$r^2$
VB <sup>b</sup>	0.22 (0.18–0.26)	< 0.001	1.27 (0.94–1.61)	< 0.001	0.55
GVB	0.16 (0.11–0.21)	< 0.001	0.92 (0.70–1.14)	< 0.001	0.59
<b><math>L_O</math> (m)</b>					
VB	$2.18 \times 10^{-3}$ (-1.08–1.52) $\times 10^{-2}$	0.736	0.52 (0.39–0.64)	< 0.001	0.62
GVB	$6.59 \times 10^{-4}$ (-1.37–1.50) $\times 10^{-2}$	0.927	0.60 (0.44–0.76)	< 0.001	0.56
<b><math>R_T</math></b>					
-	0.20 (0.07–0.33)	0.003	0.75 (0.60–0.90)	< 0.001	0.66
<b><math>R_D</math></b>					
VB	0.47 (0.32–0.63)	< 0.001	0.22 (-0.07–0.51)	0.140	0.05
GVB	0.20 (0.00–0.40)	0.052	0.66 (0.32–1.00)	< 0.001	0.25

4 Linear functions of the form  $y = ax + b$  were fit to observations of geometric attributes:  $A_D$  (%), the  
 5 percent of total damaged cross-sectional area;  $L_O$  (m), the offset length between the centroid of the  
 6 trunk and the centroid of the largest damaged part; and  $R$  (dimensionless), the roundness of the trunk,  
 7  $R_T$ , and largest damaged part,  $R_D$ .

8 <sup>b</sup>For each sonic tomogram, either violet and blue (VB) or green, violet, and blue (GVB) was used to  
 9 select damaged parts. In a PicCUS® sonic tomogram, the four colors used to visualize acoustic  
 10 transmission speeds and the corresponding internal wood condition are as follows: brown, solid;  
 11 green, intermediate; violet, damaged; and blue, damaged.  
 12



1 Table 4: Analysis of variance of the effect of mathematical methods and colors used to select  
 2 damaged parts on the absolute difference (%) between maximum  $Z_{LOSS}$  determined using sonic  
 3 tomograms and binary images of the destructively measured internal condition of trees

<b>Effect<sup>a</sup></b>	<b>df</b>	<b>F</b>	<b>p</b>	<b>Level</b>	<b>LS Mean (SE)<sup>b</sup></b>
Colors	1, 700	41.77	< 0.001	VB	0.23 (0.01)a
				GVB	0.17 (0.01)b
Methods	6, 700	13.42	< 0.001	Ciftci I(a)	0.16 (0.01)a
				Ciftci I(b)	0.19 (0.01)a
				Ciftci I(c)	0.17 (0.01)a
				Ciftci II	0.19 (0.01)a
				Coder	0.27 (0.01)b
				<i>zloss</i>	0.16 (0.01)a
				Wagener	0.24 (0.01)b
Colors × Methods	6, 700	0.53	0.785		

4 <sup>a</sup>Fixed effects include mathematical methods used to estimate  $Z_{LOSS}$  from sonic tomograms: Ciftci I(a),  
 5 Ciftci I(b), Ciftci I(c), Ciftci II, Coder, Numerical, and Wagener; colors used to select damaged parts  
 6 in sonic tomograms: violet and blue (VB) and green, violet, and blue (GVB); and their interaction:  
 7 methods × colors. See the accompanying text for more information about the various mathematical  
 8 methods used to compute  $Z_{LOSS}$ .

9 <sup>b</sup>Least squares (LS) means followed by the same letter are not significantly different at the  $\alpha = 0.05$   
 10 level.

11

1 Table 5: Analysis of covariance of the effect of mathematical methods on the absolute difference (%)  
 2 between maximum  $Z_{LOSS}$  determined using sonic tomograms and binary images of the destructively  
 3 measured internal condition of trees, after accounting for geometric features of the examined cross  
 4 sections

Effect <sup>a</sup>	df	<i>F</i>	<i>p</i>	Level	Parameter estimate (95% CI)	<i>p</i>
Method	7, 664	2.07	0.045	Ciftci I(a)	0.02 (-0.020–0.062)	0.308
				Ciftci I(b)	0.01 (-0.029–0.052)	0.582
				Ciftci I(c)	0.02 (-0.025–0.057)	0.447
				Ciftci II	0.04 (-0.006–0.076)	0.093
				Coder	0.07 (0.031–0.113)	0.001
				<i>zloss</i>	0.04 (-0.006–0.076)	0.097
				Wagener	0.03 (-0.010–0.072)	0.136
				<i>A<sub>D</sub></i> (error)	1, 664	116.59
<i>L<sub>O</sub></i> × Method	7, 664	26.74	< 0.001	Ciftci I(a)	0.51 (0.153–0.868)	0.005
				Ciftci I(b)	1.02 (0.661–1.376)	< 0.001
				Ciftci I(c)	0.72 (0.362–1.077)	< 0.001
				Ciftci II	0.72 (0.360–1.075)	< 0.001
				Coder	1.32 (0.959–1.674)	< 0.001
				<i>zloss</i>	0.34 (-0.023–0.692)	0.067
				Wagener	1.43 (1.073–1.788)	< 0.001

5 <sup>a</sup>Fixed effects include mathematical methods used to estimate  $Z_{LOSS}$  from sonic tomograms: Ciftci I(a),  
 6 Ciftci I(b), Ciftci I(c), Ciftci II, Coder, Numerical, and Wagener See the accompanying text for more  
 7 information about the various mathematical methods used to compute  $Z_{LOSS}$ . Covariates include  
 8  $A_D$ (error) (%), the absolute difference between the percent of total damaged cross-sectional area  
 9 measured using tomograms and binary images of the destructively measured internal condition of  
 10 trees, and  $L_O$  (m), the offset length between the centroid of the trunk and the centroid of the largest  
 11 damaged part. The form of the associated model is  $y_{ij} = \alpha_i + \beta_i w + \gamma x + e_{ij}$ , where  $\alpha_i$  denotes the  
 12 intercept of the  $i^{\text{th}}$  mathematical method,  $\beta_i$  denotes the slope of the  $i^{\text{th}}$  mathematical method with  
 13 respect to the covariate  $w$  ( $L_O$ ),  $\gamma$  denotes the overall slope with respect to the covariate  $x$  [ $A_D$ (Error)],  
 14 and  $e_{ij}$  denotes the experimental unit error.  
 15

1 Table 6: Mean separation for the analysis of covariance of the effect of mathematical methods on the  
 2 absolute difference (%) between maximum  $Z_{Loss}$  determined using sonic tomograms and binary  
 3 images of the destructively measured internal condition of trees, determined at six combinations of  
 4 two covariates accounting for geometric features of the examined cross sections

<b>Method</b>	$A_D(\text{Error})^a$ 0			0.4		
	$L_o$ 0	0.13	0.25	0	0.13	0.25
Ciftci I(a)	0.02 (0.02)a	0.09 (0.02)ab	0.15 (0.03)ab	0.21 (0.02)a	0.27 (0.02)ab	0.33 (0.03)ab
Ciftci I(b)	0.01 (0.02)a	0.14 (0.02)b	0.27 (0.03)bc	0.20 (0.02)a	0.33 (0.02)b	0.45 (0.03)bc
Ciftci I(c)	0.02 (0.02)a	0.11 (0.02)ab	0.20 (0.03)ab	0.20 (0.02)a	0.30 (0.02)ab	0.38 (0.03)ab
Ciftci II	0.04 (0.02)a	0.13 (0.02)ab	0.21 (0.03)ab	0.22 (0.02)a	0.31 (0.02)ab	0.40 (0.03)ab
Coder	0.07 (0.02)a	0.24 (0.02)c	0.40 (0.03)d	0.26 (0.02)a	0.43 (0.02)c	0.59 (0.03)d
<i>zloss</i>	0.03 (0.02)a	0.08 (0.02)a	0.12 (0.03)a	0.22 (0.02)a	0.26 (0.02)a	0.30 (0.03)a
Wagener	0.03 (0.02)a	0.22 (0.02)c	0.39 (0.03)cd	0.22 (0.02)a	0.40 (0.02)c	0.57 (0.03)cd

5 <sup>a</sup>Covariates include  $A_D(\text{error})$  (%), the absolute difference between the percent of total damaged cross-  
 6 sectional area measured using tomograms and binary images of the destructively measured internal  
 7 condition of trees, and  $L_o$  (m), the offset length between the centroid of the trunk and the centroid of  
 8 the largest damaged part. Within each column, least squares (LS) means followed by the same letter  
 9 are not significantly different at the  $\alpha = 0.05$  level.

10